

Electron-correlation effects in the photoionization of N_2

R. E. Stratmann, Gunadya Bandarage, and Robert R. Lucchese

Department of Chemistry, Texas A&M University, College Station, Texas 77843-3255

(Received 5 December 1994)

We have implemented a multichannel configuration-interaction complete-active-space (MCCI CAS) approximation to study electron-correlation effects in molecular photoionization. This approach includes both target relaxation and correlation due to coupling between different asymptotic scattering channels. The method employs a complete-active-space configuration-interaction wave function to represent the bound target states where the configuration interaction is computed using a single-center expansion to evaluate all integrals. The scattering equations are then solved using the Schwinger variational method. We present results of a detailed MCCI-CAS-Schwinger study of the photoionization of molecular nitrogen in the photon energy region of 19–26 eV, including nine coupled electronic channels. The results are in good agreement with the available experimental data. In particular, we obtain theoretical cross sections including interactions with the ionization channel leading to the $C^2\Sigma_u^+$ state of N_2^+ . The theoretical results are found to have a resonance structure similar to that observed in the experimental photoelectron asymmetry parameters in the $(3\sigma_g)^{-1}$ ionization channel near 22 eV.

PACS number(s): 33.80.Eh, 33.60.Cv, 03.65.Nk

I. INTRODUCTION

In recent years, angle-resolved photoelectron spectroscopy has provided a wealth of information for probing the electronic structure of small molecules, both for molecules in the gas phase and molecules adsorbed on surfaces. The interpretation of many aspects of the available data represents a formidable challenge to theory. Even though current theory is, in general, quite good for small systems, there are still qualitative and quantitative discrepancies between theory and experiment. The foremost example, where there are still discrepancies, is the photoionization of N_2 , which has been studied by numerous theoretical [1–8] methods and has also been the object of many experimental studies [9–13].

The main questions that remain and that we wish to examine are what degree of correlation is necessary and how many (and which) ion states must be included to accurately represent the valence photoionization of molecular N_2 . Recent calculations [1] using the separated-channel frozen-core Hartree-Fock (SCFCHF) and the multichannel frozen-core Hartree-Fock (MCFCHF) approximations indicate that in general the MCFCHF results are in better agreement with experiment. However, there are certain quantitative aspects of the experimental cross sections that are better reproduced by the much simpler SCFCHF results. Thus, for example, MCFCHF results do not have the intensity in the $1\pi_u \rightarrow k\pi_g$ continuum channel which wrongly presents itself as a strong valence transition above threshold in SCFCHF calculations, and by including the important interchannel coupling effects, the MCFCHF calculations yield the structure in the $(2\sigma_u)^{-1}$ photoelectron asymmetry parameter found experimentally near 33 eV. However, even though the qualitative features of the computed cross sections are improved by considering the effects of interchannel coupling, quantitative agreement is made worse in some channels as exemplified by the fact that the SCFCHF re-

sults give better agreement with the experiments for the width and position of the shape resonance in the $(3\sigma_g)^{-1}$ ionization channel. Thus, there must be important deficiencies in the treatment of correlation effects in the MCFCHF calculations; this is also indicated by the lack of agreement in the length and velocity forms in the cross sections of the $(1\pi_u)^{-1}$ channel.

There exist further significant deviations between theory and experiment as exemplified in the photoelectron asymmetry parameter in the $(3\sigma_g)^{-1}$ channel [10] near 22 eV which is due to autoionization leading to the $C^2\Sigma_u^+$ state of N_2^+ which was not included in the MCFCHF calculation, thus indicating the need to include additional ion states.

In the close-coupling approximation for studying photoionization, the total N -electron wave function is expanded as a sum of antisymmetrized, spin-adapted products of $(N-1)$ -electron target configuration state functions (CSF) and single-electron channel orbitals. This formalism includes effects due to target relaxation, correlation, and polarization as well as interchannel coupling. However, to date, little work has been done in using multiconfigurational target wave functions for e -molecule scattering or molecular photoionization [14–18].

We have recently reported a multiconfigurational multichannel Schwinger study [14] on the core ionization of CO. In that study, the simultaneous ionization and excitation of target electrons (shake-up processes) is an important electron correlation effect that cannot be described by the frozen-core model. The computational method used then was severely limited; only CSF's that had three or fewer singly occupied orbitals could be included. Thus, in the construction of a singlet N -electron wave function from $(N-1)$ -electron doublet CSF's that contain three or fewer singly occupied orbitals, there exist only three different cases that need to be considered (Table I). These three cases are easily identified and coded. However, as the number of singly occupied orbitals

TABLE I. Form of the $(N-1; S=1/2, M_S=1/2)$ and $(N; S=0, M_S=0)$ -electron CSF's for some simple cases.

Wave function	CSF	Path
ψ_1	$A[(\text{core})\phi_a\{\alpha\}]$	+1
ψ_2	$\frac{A}{\sqrt{6}}[(\text{core})\phi_a\phi_b\phi_c\{2\alpha\alpha\beta-\beta\alpha\alpha-\alpha\beta\alpha\}]$	+1+1-1
ψ_3	$\frac{A}{\sqrt{2}}[(\text{core})\phi_a\phi_b\phi_c\{\alpha\beta\alpha-\beta\alpha\alpha\}]$	+1-1+1
$\psi_1(\chi_i)$	$\frac{A}{\sqrt{2}}[(\text{core})\phi_a\chi_i\{\alpha\beta-\beta\alpha\}]$	+1-1
$\psi_2(\chi_i)$	$\frac{A}{\sqrt{12}}[(\text{core})\phi_a\phi_b\phi_c\chi_i\{2\alpha\alpha\beta\beta-\beta\alpha\alpha\beta-\alpha\beta\alpha\beta$ $-\beta\alpha\beta\alpha-\alpha\beta\beta\alpha+2\beta\beta\alpha\alpha\}]$	+1+1-1-1
$\psi_3(\chi_i)$	$\frac{A}{2}[(\text{core})\phi_a\phi_b\phi_c\chi_i\{\alpha\beta\alpha\beta-\beta\alpha\alpha\beta-\alpha\beta\beta\alpha+\beta\alpha\beta\alpha\}]$	+1-1+1-1

increases, the number of cases that need to be considered grows rapidly, the work needed to implement these on a case by case basis becomes overwhelming. Further, such an approach would not be general, a new set of cases would need to be programmed for every different final spin symmetry that one encounters in different spin species (e.g., molecular oxygen or ionized radicals).

Here we present a more general approach that allows the inclusion, in principle, of any level of excitation. We have also extended the code to take full advantage of all symmetry aspects.

There are several objectives for the current work. First, by including more CSF's with more unpaired electrons we hope to obtain significant improvements by accurately describing the residual ion. In particular, we expect quantitative improvements, such as bringing the length and velocity form into better agreement, as well as qualitative improvements in the calculated cross sections and photoelectron asymmetry parameters by including more accurately described ion states.

Previously, all integrals used in the computation of the $(N-1)$ -electron target states were obtained analytically using standard quantum-mechanical codes. However, in the N -electron scattering problem all integrals are done numerically. This leads to small off-diagonal channel matrix elements that were neglected in our previous study [14]. The second objective was to avoid this problem by treating the bound and continuum part of the problem on an equal footing (i.e., numerically).

The number of target states included in the close-coupling calculations is necessarily limited due to practical considerations. It has been pointed out that, when using multiconfigurational targets, the exclusion of some of the energetically open channels can give rise to spurious resonances [18]. This effect can be illustrated by considering a case where there is a compact representation of the included target states, such that each state contains one identifiable principal configuration. The continuum function can develop a component that resembles a penetration term that can be represented by an L^2 expansion, and the penetration term is thus built exclusively from N -electron target orbitals used in the close-coupling expansion. The same penetration term can arise from different channels. In particular, the penetration term

might represent a major component of one of the omitted ion state channels, i.e., can be identified with an $(N-1)$ -electron eigenstate, thereby leading to a spurious resonance. One solution that has been proposed to solve this problem consists of orthogonalizing the channel scattering states to the strongly occupied molecular orbitals. This solution is good only for states with an identifiable principal configuration such that the orbital set can be divided into strongly doubly occupied and weakly occupied orbitals; this approach will not work for highly correlated states.

However, such penetration terms can only give rise to states that are included in a complete-active-space configuration interaction (CASCI). The third objective was to illustrate the utility of the CAS approach since no spurious resonances can occur if one includes all energetically open channels obtained from the CAS. However, the number of open channels to be included using a finite basis set, rises rapidly as the incident photon energy reaches the ionization energy, thereby making the computation ever more demanding.

We will consider the photoionization process in the fixed nuclei approximation, and limit ourselves to consider only the ionization from the valence orbitals of N_2 and to the restricted photon energy region of 19–26 eV where there are few enough open channels to make the calculation feasible.

II. THEORY

The multichannel configuration-interaction (MCCI) wave function for a system of N electrons at a total energy where one electron is asymptotically free can be written as [19]

$$\Psi_S^{\text{MCCI}} = \sum_{i=1}^{N_c} \Phi_i(\chi_{i,S}) = \sum_{i=1}^{N_c} \sum_{j=1}^{N_b} \psi_j(\chi_{i,S}) C_{ji}, \quad (1)$$

where $\chi_{i,S}$ is the i th channel scattering function, ψ_j is an $(N-1)$ -electron channel CSF, Φ_i represents the configuration-interaction wave function of the residual target in channel i , N_c is the number of channels, and N_b is the number of CSF's used in the expansion. The notation $\psi_j(\chi_{i,S})$ implies an antisymmetrized spin-adapted

N -electron CSF constructed from the product of ψ_j and $\chi_{i,S}$.

In any given channel, we consider all possible excitations consistent with the total M value and g/u symmetry of some given reference configuration.

We next construct all the linearly independent spin eigenfunctions arising from a given spatial orbital occupation [20]. We note that the spin operators S^2 and S_z are symmetric under a permutation of the particles, hence a pure spin eigenfunction remains a spin eigenfunction under permutation with the same values of S and M . Thus, the construction of spin eigenfunctions can be isolated from any considerations of the orbital form of the wave function, and also from the overall space-spin antisymmetry requirements. Thus, if one takes any orbital product and attaches a spin eigenfunction and antisymmetrizes, the result will be a properly antisymmetric spin eigenfunction. Since the spin eigenfunctions consist of products of spin functions, the antisymmetrizer will turn every term into a Slater determinant constructed from the spin orbitals which are products of the spatial orbitals and spin functions.

To obtain the actual spin functions $X(N, S, M)$ we have used the branching diagram method [20]. Since the Hamiltonian and the other physical quantities we are interested in are spin independent we may choose $M=S$. In the branching diagram method (Fig. 1), starting with an (n_q-1) -electron spin eigenfunction with quantum number S , two n_q -electron spin eigenfunctions can be formed by either adding the spin of the n_q th electron leading to the state with total spin $S+1/2$, or by subtracting it to obtain the state with total spin $S-1/2$ (for $S \geq 1/2$), according to the addition theorem of angular momentum. Starting with a single electron, one successively adds or subtracts the spin of additional electrons, the sequence of additions and subtraction defining a path, which is easily represented by a string of integers, $\{\pm 1\}$. For a given final N one must find all possible paths leading to the state with spin S . For the explicit construction

of a spin eigenfunction, using the notation $S^\pm = S \pm 1/2$, the proper linear combinations for subtraction is given by [20]

$$X(n_q, S) = [(2S+1)(2S+2)]^{-1/2} \times [-S^* S_+(n_q) + (2S+1)1] \times X(n_q-1, S^+) \beta(n_q), \quad (2)$$

where S_\pm are the usual spin raising and lowering operators, and where

$$S^*(a) = \sum_{i=1}^{n_q-1} S_-(i) \quad (3)$$

and the proper linear combinations for addition is given by

$$X(n_q, S) = X(n_q-1, S^-) \alpha(n_q). \quad (4)$$

Thus, for a given spatial orbital occupation q , the $(N-1)$ -electron CSF can then be written as

$$\psi_{q_i}^\pm = Aq\{\pm 1\}_i = AqX_i(N-1, S^\pm) \quad (5)$$

and the N -electron CSF is written as

$$\psi_{q_i}(\chi_k) = Aq\chi_k\{\pm 1\}'_i = Aq\chi_k X_i(N, S), \quad (6)$$

where A is the antisymmetrizer, q represents a set of occupation number, and the path $\{\pm 1\}$ and $\{\pm 1\}'$ differ only by an additional integer in the latter.

We have also implemented a procedure to construct Σ states ($m=0$) with the proper symmetry with respect to reflection in the plane containing the intermolecular axis. Under this symmetry operation (we take the reflection plane to be the x - z plane), a spatial one-electron orbital ϕ_i is transformed into $\pm\phi_i$, and thus the entire CSF is also transformed. We then determine the overlap matrix between the original CSF and the transformed CSF which is thus the matrix representation of the symmetry operation. We then block factor and diagonalize the resulting blocks. The eigenvalues of this matrix have unit norm and the eigenvectors form a set of functions that are of the correct symmetry and are mutually orthogonal. This is a necessary procedure in order to obtain a set of CSF's that are mutually orthogonal and thus avoid linear dependence in the final CSF's.

Once we have constructed the $(N-1)$ -electron CSF's, we perform a numerical CI using our single-center-expansion scattering code to evaluate all needed integrals. From the branching diagram method, or from Eqs. (5) and (6), one can easily see that for a given spin symmetry of the N -electron wave function there is a one-to-one correspondence between the CSF's used to construct the N -electron wave function and the $(N-1)$ -electron CSF's used to construct the target states. Thus, the CI expansion coefficients C_{ji} for a given CSF $\psi_j(\chi_i)$ in the N -electron state $\Phi_i(\chi_i)$, is identical to the CI expansion coefficient for the corresponding CSF ψ_j in the $(N-1)$ -electron state Φ_i . Thus,

$$\Phi_i = \sum_j \psi_j C_{ji}, \quad (7)$$

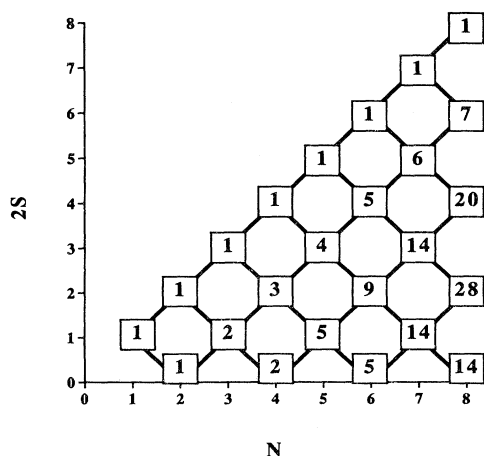


FIG. 1. Branching diagram for spin eigenfunctions. N is the number of open-shell electrons and S is the total spin angular momentum.

where the values of C are identical to those used in Eq. (1).

To make the correct association between N and $(N-1)$ -electron CSF's, for any given N -electron CSF, one must determine whether the last (continuum) electron was coupled in by addition or by subtraction. This is easily done by examining the path used to construct it. Alternatively, from Eqs. (2) and (4), it is evident that if in a given N -electron CSF there exists no determinant where the spin of the continuum electron is β (i.e., all α) then this particular N -electron CSF comes from an $(N-1)$ -electron CSF with spin S^- . Similarly, if in the N -electron CSF there exists at least one determinant where the continuum electron has spin β , then this would correspond to a CSF obtained from an $(N-1)$ -electron CSF with spin S^+ .

To obtain the scattering equations for the scattering orbital χ_i , the MCCI wave function is required to satisfy the projected Schroedinger equation

$$\left\langle \sum_{i=1} \Phi_i(\delta\chi_i) | H_N - E | \Psi_{\text{MCCI}} \right\rangle = 0, \quad (8)$$

where H_N is the usual N -electron Hamiltonian and $\Phi_i(\delta\chi_i)$ represents all possible variations of $\Phi_i(\chi_i)$ which can be obtained by varying the scattering orbital χ_i . We do not impose any orthogonality constraints (*a priori*) between χ_i and those spatial molecular orbitals $\{\phi_j\}$ which are not doubly occupied in every configuration. This permits the scattering function to include the functional space spanned by the molecular orbitals. There exist other methods that require the scattering function to be orthogonal to the bound states [18]. To relax this unphysical restriction they include "penetration" terms that belong to the Hilbert space of L^2 N -electron wave functions. Both formulations give rise to unphysical spurious resonances when one includes only a restricted set of channel state functions. In the present calculation, however, this is avoided by including all the open channels from a CASCI calculation of the ion states in the energy range considered.

The actual computation of the potential is done as follows. Since each CSF is a sum of Slater determinants, the matrix elements of the Hamiltonian in the channel basis is expanded in a summation of matrix elements over Slater determinants. In order to apply the Condon-Slater rules to evaluate the matrix elements, the scattering function is further expanded in the molecular orbital basis set and the part orthogonal to them. This is done by inserting unity, $1 = P + Q$, where the projection operators are defined as

$$P = 1 - Q = 1 - \sum_{i=1} |\phi_i\rangle\langle\phi_i| \quad (9)$$

and where the sum runs over all active spin orbitals. Each matrix element is thus reduced to sums of the usual one and two electron integrals and products of overlaps with one and two electron integrals. The general form of this potential has been discussed in detail by Bandarage and Lucchese [14].

III. RESULTS AND DISCUSSION

A self-consistent-field (SCF) calculation on the ground state of N_2 using the standard triple ζ valence plus polarization basis set [21] at an internuclear separation of 2.068 a.u. gives a total electronic energy of $-108.977\,829$ a.u. The SCF initial state of molecular nitrogen, including the two lowest-lying virtual orbitals is given by

$$(1\sigma_g)^2(1\sigma_u)^2(2\sigma_g)^2(2\sigma_u)^2(3\sigma_g)^2(1\pi_u)^4(1\pi_g)^0(3\sigma_u)^0.$$

The canonical molecular orbital basis so obtained usually leads to a slowly convergent CI expansions due to the fact that the virtual orbitals are too diffuse. Thus it is useful to employ a set of natural orbitals to keep N_b , the length of the CSF expansion, to a minimum. We have then included correlation through a CAS-MCSCF calculation using the 10 orbitals listed above where we have maintained the $1\sigma_g$ and $1\sigma_u$ orbitals as doubly occupied in all configurations and considered all other orbitals active. The CAS-MCSCF total energy is $-109.127\,082$ a.u. We then obtain a set of natural orbitals by diagonalizing the one-electron density matrix for this state. The initial state CAS-MCSCF wave function consists of 96 symmetry adapted CSF's.

After construction of the $(N-1)$ -electron CSF's we perform a numerical CASCI using matrix elements computed using the single-center expansion technique. We are primarily interested in obtaining good excitation energies and not absolute ionization potentials (IP's). Thus we present in Table II the energies for the three lowest valence excited states of N_2^+ relative to the ground state of N_2^+ . We have considered the dependence of the IP's on the l expansion using expansions up to $l=100$ and $l=40$. We have verified that the differences in the excitation energies using the different expansions are within 0.2 eV. We have previously reported that the shape resonance for ionization in the $(3\sigma_g)^{-1}$ channel is relatively insensitive of the maximum l used [22]. Thus, to minimize the computational effort required and to insure a reasonable accuracy of the calculation, all calculations presented below were done using an expansion up to $l=40$. The total energy is $-108.291\,819$ a.u. for N_2 and $-107.694\,987$ a.u. for N_2^+ using $l=40$. Thus, we compute the lowest-lying IP at 16.24 eV, which is 0.64 eV above the experimentally determined first IP of 15.60 eV.

The vertical IP for the $C^2\Sigma_u^+$ of N_2^+ is some 3 eV above the experimentally observed adiabatic IP. In a simple molecular orbital picture, this state represents a shake-up state in which a bonding electron σ_g electron is

TABLE II. Excitation energies (in eV) from the ground ion state of N_2^+ to the three lowest ion states.

Transition	MCEP		Experiment
	Ref. [25]	CASCI $l=40$	
$A^2\Pi_u^+ \leftarrow X^2\Sigma_g^+$	1.72	1.06	1.38
$B^2\Sigma_u^+ \leftarrow X^2\Sigma_g^+$	3.04	2.43	3.18
$C^2\Sigma_u^+ \leftarrow X^2\Sigma_g^+$	10.79	10.58	9.8 ^a

^aEstimated from RKR potential (Ref. [23]).

promoted to the antibonding π_g orbital and is accompanied by a considerable increase in bond length; the experimentally determined internuclear equilibrium distances [24] are 1.097 68 Å or $X^1\Sigma_g^+$ and 1.471 Å for $C^2\Sigma_u^+$. Thus, the difference between the computed vertical IP and the experimental IP is in qualitative agreement with our expectations.

In the photoionization calculations the highest-lying open channel corresponds to the $B^2\Sigma_u^+$ state of N_2^+ . Since the computed IP is within 0.1 eV of the experimentally determined vertical IP for this state, we have decided not to shift any of our IP's and, therefore, present a completely *ab initio* calculation.

We present in Table III our results for the lowest-lying ion states of N_2^+ . We compare our results to results obtained from the GAMESS computer program [21]. The results presented there should be identical to our own in the limit that the l expansion approaches infinity. We have verified that for $l=100$ agreement is within 0.02 eV. We have also compared our results to the multiconfiguration electron propagator (MCEP) results of Nichols, Yeager, and Jørgensen [25] and have found that all IP's computed here are within 1 eV of those found using MCEP. We further present the orbital occupation differences between the Hartree-Fock (HF) neutral-target wave function and the principal CSF's of the ion states. Some of the configurations have the same primary configuration and differ by their spin symmetry in the π subsystem to form intermediate singlets or triplets.

After the three ion hole states, all other states shown, represent shake-up states in which one of the electrons has been promoted to the π_g^* orbital and roughly appear

in the order as expected in a simple molecular orbital picture. Thus, states in which the π subsystem is spin coupled to give an intermediate triplet lie energetically lower, in agreement with Hund's rule. We further note that there is a large splitting when the two unpaired electrons lie in the same plane (i.e., same m value) thus having stronger e^-e^- interactions.

We have performed MCCI-CAS calculations including the first 3 (MCCI-CAS-3), the first 4 (MCCI-CAS-4), and the first 9 (MCCI-CAS-9) ion states listed in Table III. We will further present results in the SCFCHF approximation and the MCFCHF approximation previously obtained [1]. In the MCFCHF calculation, the target states were the four valence ion states $(3\sigma_g)^{-1}2\Sigma_g^+$, $(1\pi_u)^{-1}2\Pi_u^+$, $(2\sigma_u)^{-1}2\Sigma_u^+$, and $(2\sigma_g)^{-1}2\Sigma_g^+$, which were represented by single CSF wave functions constructed from the SCF orbitals of the ground state of N_2 . In the present MCCI-CAS calculations, we have computed points every 0.1 eV. In all regions where we could detect any structure we have done points at every 0.05 eV.

In Fig. 2, we present the total cross sections for the $(3\sigma_g)^{-1}$ channel. We present results obtained in the SCFCHF, MCFCHF, and MCCI-CAS-9 calculations with available experimental data. The main feature in this ionization channel is due to the shape resonance centered at about 29 eV in the $3\sigma_g \rightarrow k\sigma_u$ channel and which determines the overall appearance of the cross sections as can be seen from the SCFCHF. In the energy range considered, the SCFCHF and MCFCHF calculations are in good agreement with each other. The MCCI-CAS-9 calculations presents two prominent peaks at approximately 20.5 and 23.5 eV which are not clearly

TABLE III. The ionization potentials (in eV) for ion states of N_2^+ below 33 eV. The last column lists the occupational difference between the HF neutral target and the principal occupation of the ion state.

Ion State	CASCI $l=40$	GAMESS Ref. [21]	MCEP Ref. [25]	Principal configuration
States included in the MCCI-CAS-9 scattering calculation				
1 $2\Sigma_g^+$	16.24	16.25	15.52	$(3\sigma_g)^{-1}$
2 $2\Pi_u$	17.30	17.29	17.24	$(1\pi_u)^{-1}$
3 $2\Sigma_u^+$	18.67	18.83	18.56	$(2\sigma_u)^{-1}$
4 $2\Sigma_u^+$	26.82	26.82	26.31	$(3\sigma_g)^{-1}(1\pi_u)^{-1}(1\pi_g)^{+1}$
5 $2\Pi_g$	26.79	26.87	26.73	$(3\sigma_g)^{-2}(1\pi_g)^{+1}$
6 $2\Pi_g$	27.16	27.14	26.82	$(1\pi_u)^{-2}(1\pi_g)^{+1a}$
7 $2\Sigma_u^-$	27.93	27.93		$(3\sigma_g)^{-1}(1\pi_u)^{-1}(1\pi_g)^{+1}$
8 $2\Delta_u$	27.95	27.94		$(3\sigma_g)^{-1}(1\pi_u)^{-1}(1\pi_g)^{+1}$
9 $2\Delta_u$	28.44	28.44		$(3\sigma_g)^{-1}(1\pi_u)^{-1}(1\pi_g)^{+1}$
Other low-lying states found in CAS-CI calculation				
$2\Phi_g$	28.56	28.54		$(1\pi_u)^{-2}(1\pi_g)^{+1}$
$2\Sigma_u^-$	28.94	28.93		$(3\sigma_g)^{-1}(1\pi_u)^{-1}(1\pi_g)^{+1}$
$2\Pi_g$	29.31	29.31	28.84	$(1\pi_u)^{-2}(1\pi_g)^{+1a}$
$2\Sigma_g^+$	29.91	30.06	29.78	$(2\sigma_u)^{-1}(1\pi_u)^{-1}(1\pi_g)^{+1}$
$2\Pi_u$	30.42	30.61	29.59	$(2\sigma_u)^{-1}(3\sigma_g)^{-1}(1\pi_g)^{+1}$
$2\Sigma_g^-$	30.82	30.98		$(2\sigma_u)^{-1}(1\pi_u)^{-1}(1\pi_g)^{+1}$
$2\Delta_g$	31.31	31.48		$(2\sigma_u)^{-1}(1\pi_u)^{-1}(1\pi_g)^{+1}$
$2\Delta_g$	32.29	32.46		$(2\sigma_u)^{-1}(1\pi_u)^{-1}(1\pi_g)^{+1}$

^aPrimarily $(\pi_u)^{-1}(\pi_u)^{-1}(\pi_g)^{+1}$; strongly coupled to $(\pi_u)^{-2}(\pi_g)^{+1}$.

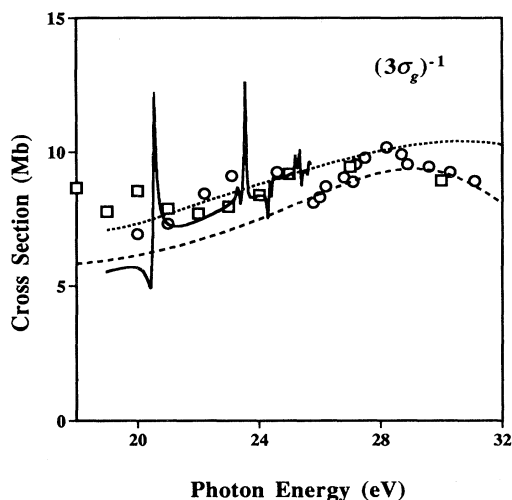


FIG. 2. Photoionization cross section in the $(3\sigma_g)^{-1}$ channel of N_2 . Mixed form for the SCFCHF, four-channel MCFCHF, and nine-channel MCCI-CAS-9 calculations with comparison to experiment: (—) MCCI-CAS-9 mixed form; (····) MCFCHF four-channel mixed form; (---) SCFCHF mixed form; (□) experimental data from Hamnett, Stroll, and Brion (Ref. [9]); (○) experimental data of Plummer *et al.* (Ref. [10]).

indicated by experiment.

In Fig. 3, we present the photoelectron asymmetry parameter for this channel. Near threshold, the MCCI-CAS-9 calculation agrees much better with the available experimental data than either the SCFCHF or the MCFCHF calculations. However, it presents a prominent structure at 20.5 and 23.5 eV, whereas the experi-

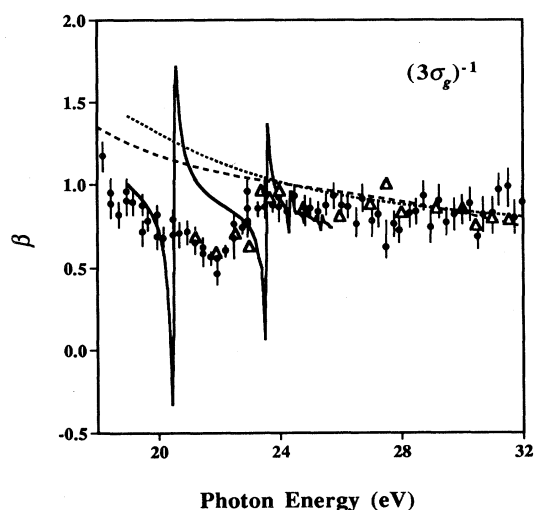


FIG. 3. Photoelectron asymmetry parameter for the $(3\sigma_g)^{-1}$ channel of N_2 . Mixed form for the SCFCHF, four-channel MCFCHF, and nine-channel MCCI-CAS-9 calculations with comparison to experiment: (—) MCCI-CAS-9 mixed form; (····) MCFCHF four-channel mixed form; (---) SCFCHF mixed form; (Δ) experimental data of Marr *et al.* (Ref. [12]); (●) experimental data of Southworth *et al.* (Ref. [11]).

ment clearly indicates a large broad dip centered around 22 eV. To investigate this further, we also present in Fig. 4 a comparison of the asymmetry parameter obtained from various MCCI-CAS calculations including three, four, and nine channels. The MCCI-CAS-3 calculation represents essentially a horizontal line, in better agreement with experiment than either the SCFCHF or the MCFCHF calculations. The MCCI-CAS-3 calculation is equivalent to the MCFCHF calculation except that it uses correlated target states. Thus, this is indicative that correlation has significantly improved the calculation.

The MCCI-CAS-4 calculation which further included the $C^2\Sigma_u^+$ state yields a resonance at approximately 22 eV in agreement with experiment although it is somewhat narrower. It is to be expected that vibrational averaging will be important for obtaining a better agreement with experiment. However, it is not clear if the current calculation treats the fixed nuclei photoionization problem with sufficient accuracy to obtain quantitative agreement upon vibrational averaging. We have determined that the MCCI-CAS-4 calculation leads to very good agreement in all channels for both the cross section and the asymmetry parameter, although perhaps for the wrong reasons.

The most accurate MCCI-CAS-9 channel calculation however leads to somewhat different conclusions as it indicates additional significant structure. By comparing the cross section and asymmetry parameters in all channels for both the MCCI-CAS-4 and -9 channels results some general remarks can be made. First, there is a new prominent feature at 23.5 eV in the nine-channel calculation. Second, the structure due to inclusion of the $C^2\Sigma_u^+$ state centered around 22 eV in the four-channel calculation is moved down some 1–2 eV in the nine-channel calculation presumably due to strong coupling to the feature at 23.5 eV.

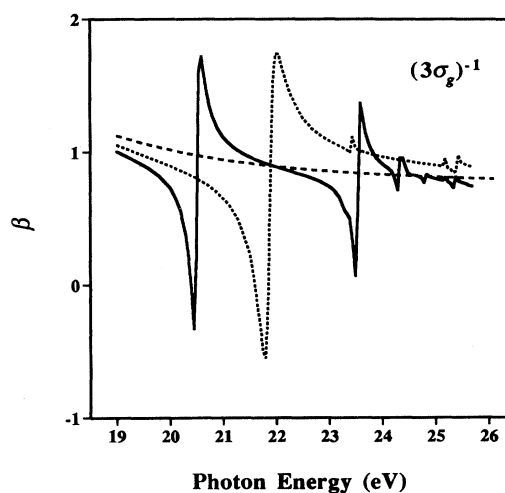


FIG. 4. Photoelectron asymmetry parameter for the $(3\sigma_g)^{-1}$ channel of N_2 . Mixed form for the three-channel MCCI-CAS-3, four-channel MCCI-CAS-4, and nine-channel MCCI-CAS-9 calculations: (—) MCCI-CAS-9 mixed form; (····) MCCI-CAS-4 mixed form; (---) MCCI-CAS-3 mixed form.

Thus, even though the MCCI-CAS-4 calculation is in excellent agreement with experiment, it becomes apparent that the structure that is observed experimentally near 22 eV is probably not due exclusively to the $C^2\Sigma_u^+$ state. The difference between the MCCI-CAS-4 and MCCI-CAS-9 results indicate strong channel coupling and correlation effects which are probably not converged with respect to inclusion of more channels. Additionally, vibrational averaging might significantly change the presented results.

In Fig. 5, we present the total cross sections for the $(1\pi_u)^{-1}$ channel. We present results obtained in the SCFCHF, MCFCHF, and MCCI-CAS-9 calculations with the available experimental data of Hammer, Stoll, and Brion [9] and Plumer *et al.* [10]. In Fig. 6, we examine the difference between the length and velocity forms for this channel. We have previously pointed out [1] that in the MCFCHF approximation there exist large differences in the length and velocity forms (6–9 Mb), thus indicating significant correlation errors. The present MCCI-CAS-9 have approximately halved (5 Mb) this difference; we find the length form to be in excellent agreement with experiment. However, for the sake of consistency and simplicity we will only present results in the mixed form, which we have also found to be in reasonable agreement with experiment.

As is well known [26], in the SCFCHF approximation, the poor positioning of the π_g^* orbital in the continuum leads to a large peak at threshold due to the oscillator strength in the $1\pi_u \rightarrow k\pi_g$ channel which can be clearly seen in Fig. 5. Channel coupling dramatically affects the partial cross section by redistributing a portion of the oscillator strength over the different channels and brings these calculations into much better agreement with ex-

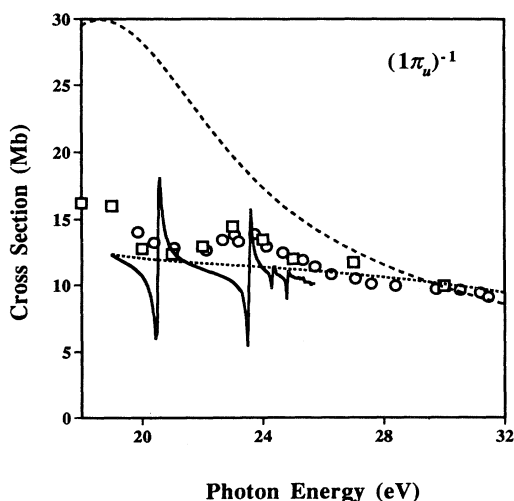


FIG. 5. Photoionization cross section in the $(1\pi_u)^{-1}$ channel of N_2 . Mixed form for the SCFCHF, four-channel MCFCHF, and nine-channel MCCI-CAS calculations with comparison to experiment: (—) MCCI-CAS-9 mixed form; (· · · ·) MCFCHF four-channel mixed form; (— — —) SCFCHF mixed form; (□) experimental data from Hammett, Stoll, and Brion (Ref. [9]); (○) experimental data of Plumer *et al.* (Ref. [10]).

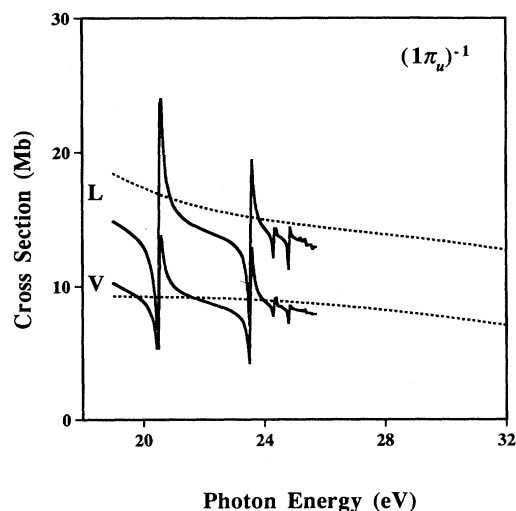


FIG. 6. Photoionization cross section in the $(1\pi_u)^{-1}$ channel of N_2 . Length and velocity forms for the MCFCHF and MCCI-CAS-9 calculations: (—) MCCI-CAS-9 length and velocity forms; (· · · ·) MCFCHF four-channel length and velocity forms.

periment. The MCFCHF and the MCCI-CAS-9 approximations are in good quantitative agreement with each other. The structure evident in the MCCI-CAS-9 results is very similar to that found in the $(3\sigma_g)^{-1}$ channel. There are two prominent features centered at 20.5 and 23.5 eV which seem to correspond roughly to the structure in the experimental data. As in the $(3\sigma_g)^{-1}$ case MCCI-CAS-4 results (not shown) indicate a single feature centered at 22 eV.

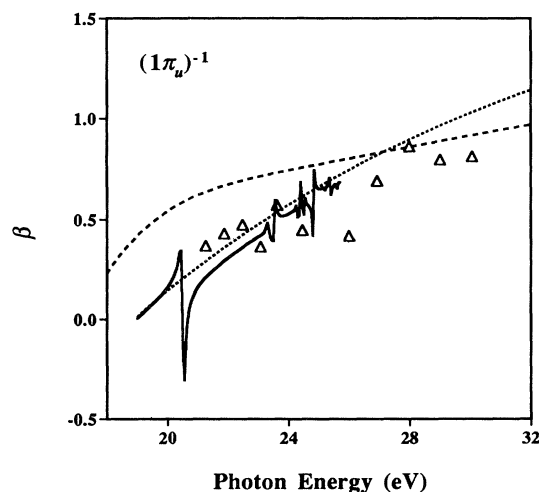


FIG. 7. Photoelectron asymmetry parameter for the $(1\pi_u)^{-1}$ channel of N_2 . Mixed form for the SCFCHF, four-channel MCFCHF, and nine-channel MCCI-CAS-9 calculations with comparison to experiment: (—) MCCI-CAS-9 mixed form; (· · · ·) MCFCHF four-channel mixed form; (— — —) SCFCHF mixed form; (△) experimental data of Marr *et al.* (Ref. [12]).

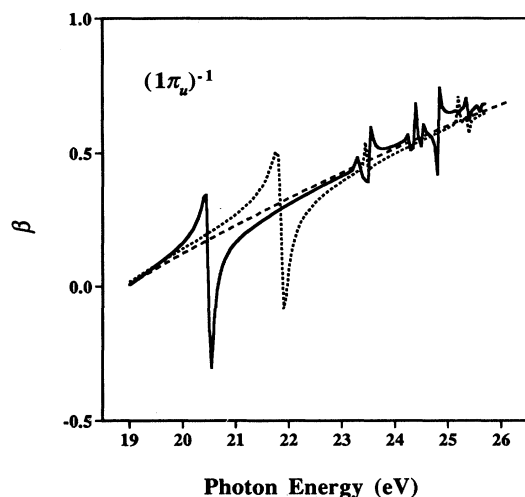


FIG. 8. Photoelectron asymmetry parameter for the $(1\pi_u)^{-1}$ channel of N_2 . Mixed form for the three-channel MCCI-CAS-3, four-channel MCCI-CAS-4, and nine-channel MCCI-CAS-9 calculations: (—) MCCI-CAS-9 mixed form; (····) MCCI-CAS-4 mixed form; (---) MCCI-CAS-3 mixed form.

In Fig. 7, we present the photoelectron asymmetry parameter for the $(1\pi_u)^{-1}$ channel. The MCCI-CAS-9 calculations seem to be in good agreement with the experimental data even though they predict a considerable structure that has not yet been resolved experimentally. We present in Fig. 8 a comparison of the different MCCI-CAS calculations including three, four, and nine channels for the asymmetry parameter in this channel. We again see the resonance at the 22 eV in the four-

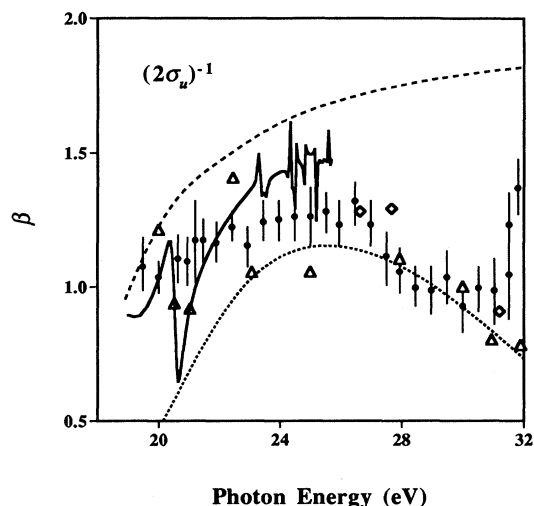


FIG. 10. Photoelectron asymmetry parameter for the $(2\sigma_u)^{-1}$ channel of N_2 . Mixed form for the SCFCHF, four-channel MCFCHF, and nine-channel MCCI-CAS-9 calculations with comparison to experiment: (—) MCCI-CAS-9 mixed form; (····) MCFCHF four-channel mixed form; (---) SCFCHF mixed form; (Δ) experimental data of Marr *et al.* (Ref. [12]); (\bullet) experimental data of Southworth *et al.* (Ref. [11]); (\diamond) experimental data of Adam *et al.* (Ref. [13]).

channel calculation which appears to be shifted to 20.5 eV in the nine-channel calculation.

In Figs. 9–11, we present our results leading to the ionization in the $(2\sigma_u)^{-1}$ channel. The SCFCHF approximation fits the experimental total cross-section data better than the MCFCHF approximation. However, the asymmetry parameters in the MCFCHF approximation

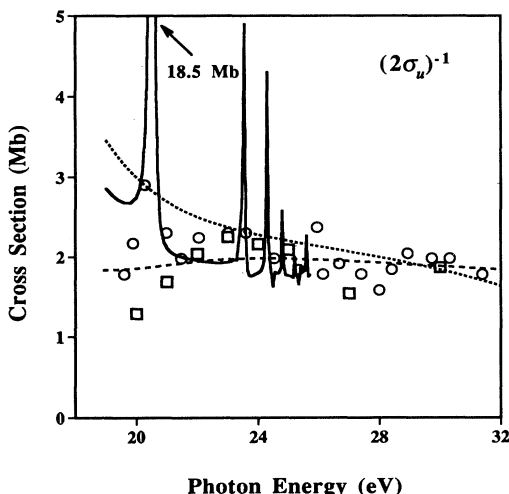


FIG. 9. Photoionization cross section in the $(2\sigma_u)^{-1}$ channel of N_2 . Mixed form for the SCFCHF, four-channel MCFCHF, and nine-channel MCCI-CAS-9 calculations with comparison to experiment: (—) MCCI-CAS-9 mixed form; (····) MCFCHF four-channel mixed form; (---) SCFCHF mixed form; (\square) experimental data from Hamnett, Stoll, and Brion (Ref. [9]); (\circ) experimental data of Plummer *et al.* (Ref. [10]).

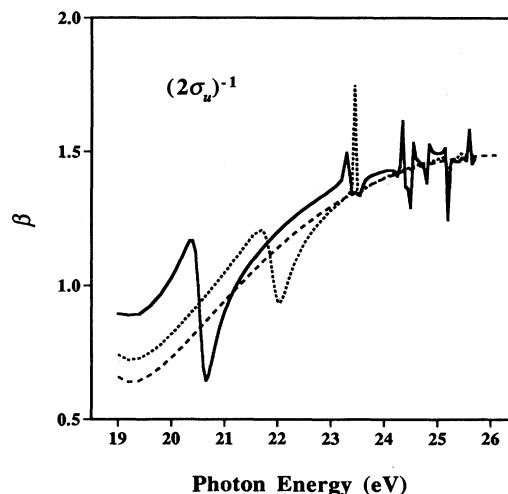


FIG. 11. Photoelectron asymmetry parameter for the $(2\sigma_u)^{-1}$ channel of N_2 . Mixed form for the three-channel MCCI-CAS-3, four-channel MCCI-CAS-4, and nine-channel MCCI-CAS-9 calculations: (—) MCCI-CAS-9 mixed form; (····) MCCI-CAS-4 mixed form; (---) MCCI-CAS-3 mixed form.

are in better agreement due to inclusion of interchannel coupling to the shape resonance in the $(3\sigma_g)^{-1}$ channel. In Fig. 9, the MCCI-CAS-9 approximation presents various maxima, the most prominent close to 20.5 eV measuring 18.5 Mb. In the MCCI-CAS-4 calculation (not shown) this peak is located close to 22 eV and measures 14.1 Mb. Thus, the structure found in this channel in the experimental total cross-section data of Plummer *et al.* [10] seems to be in better agreement with the MCCI-CAS-9 results.

The asymmetry parameter for the MCCI-CAS-9 approximations is bracketed by the SCFCHF and MCFCHF approximations and further indicate much structure that has not been resolved yet in the experimental data.

IV. CONCLUSIONS

We have studied the photoionization of N_2 using the numerical MCCI-CAS method. All the required integrals have been evaluated using a single-center expansion. Although the description of off-center core orbitals is difficult in such an expansion, by using a sufficiently large l expansion, we have obtained excitation energies that are within 0.01 eV of those obtained using analytical methods.

In the limited region where we have performed our calculation, the present results are in much better agreement with experimental results than any previous work. It would seem that the MCCI-CAS-4 results actually lead to better agreement with experiment than the more accurate MCCI-CAS-9 results. The inclusion of the $C^2\Sigma_u^+$ ion state of N_2^+ , which is present in both the above-mentioned calculations, is partly responsible for the structure centered at about 22 eV in all channels present in both the cross sections and the asymmetry parameter.

We cannot however, at this point, completely determine the extent to which the presence of this resonance explains the structure seen in the experimental data.

The choice of ion states to include in the close-coupling method is not a trivial one, since for practical reasons one can include only a limited number of channels. The inclusion of the lowest nine ion states is seen to give much structure, although agreement with experimental data is not yet completely satisfactory. Thus the calculation does not seem to be converged with respect to the number of channels that have been included. The accuracy of our results is additionally constrained by the limited orbital active space that we have used. Some of this disagreement is also certainly due to the fixed nuclei approximation used here. Including nuclear motion would probably broaden some of the structure obtained in the current calculations.

Work is currently in progress to examine some of these possible sources of disagreement. We can treat the effects of nuclear motion using numerical methods as has been demonstrated in earlier calculations [2]. We are also interested in extending this calculation to the region of 26–50 eV to investigate the correlation effects on the location and width of the $k\sigma_u$ shape resonance and on the cross sections leading to the $(2\sigma_g)^{-1}$ hole states.

ACKNOWLEDGMENTS

Before final acceptance an error in our molecular orbitals was uncovered by Robert Zurales thereby leading to the current results. We are thankful for his assistance in locating this error and for many discussions concerning these calculations. We also acknowledge partial support from the Robert A. Welch Foundation (Houston, TX) under Grant No. A-1020.

-
- [1] R. R. Lucchese and R. W. Zurales, *Phys. Rev. A* **44**, 291 (1991).
 - [2] B. Basden and R. R. Lucchese, *Phys. Rev. A* **37**, 89 (1988).
 - [3] R. R. Lucchese, G. Raseev, and V. McKoy, *Phys. Rev. A* **25**, 2572 (1982).
 - [4] M. Raoult, H. Le Rouzo, G. Raseev, and H. Lefebvre-Brion, *J. Phys. B* **16**, 4601 (1983).
 - [5] T. M. Rescigno, C. F. Bender, B. V. McKoy, and P. W. Langhoff, *J. Chem. Phys.* **68**, 970 (1978).
 - [6] P. Swanström, J. T. Golab, D. L. Yeager, and J. A. Nichols, *Chem. Phys.* **110**, 339 (1986).
 - [7] G. R. J. Williams and P. W. Langhoff, *Chem. Phys. Lett.* **78**, 21 (1981).
 - [8] S. Yabushita and C. W. McCurdy, *Phys. Rev. A* **36**, 3146 (1987).
 - [9] A. Hammett, W. Stoll, and C. E. Brion, *J. Electron Spectrosc. Relat. Phenom.* **8**, 367 (1976).
 - [10] E. W. Plummer, T. Gustafsson, W. Gudat, and D. E. Eastman, *Phys. Rev. A* **15**, 2339 (1977).
 - [11] S. H. Southworth, A. C. Parr, J. E. Hardis, and J. L. Dehmer, *Phys. Rev. A* **33**, 1020 (1986).
 - [12] G. V. Marr, J. M. Morton, R. M. Holmes, and D. G. McCoy, *J. Phys. B* **12**, 43 (1979).
 - [13] M. Y. Adam, P. Morin, P. Lablanquie, and I. Nenner (unpublished).
 - [14] Gunadya Bandarage and Robert R. Lucchese, *Phys. Rev. A* **47**, 1989 (1993).
 - [15] L. A. Colins and B. I. Schneider, in *Proceedings of the Eleventh International Conference on the Physics of Electronic and Atomic Collisions*, edited by H. Gilbody, W. Newell, F. Read, and A. Smith (North-Holland, New York, 1987).
 - [16] S. E. Branchett and J. Tennyson, *Phys. Rev. Lett.* **64**, 2889 (1990).
 - [17] A. E. Orel, T. N. Rescigno, and B. H. Lengsfeld, *Phys. Rev. A* **42**, 5292 (1990).
 - [18] B. H. Lengsfeld III and T. N. Rescigno, *Phys. Rev. A* **44**, 2913 (1991).
 - [19] R. K. Nesbet, *Variational Methods in Electron-Atom Scattering Theory* (Plenum, New York, 1980).
 - [20] R. Paunz, *Spin Eigenfunctions: Construction and Use* (Plenum, New York, 1979).
 - [21] This is the General Atomic and Molecular Electronic Structure System (GAMESS) computer codes, as described

- in M. W. Schmidt, K. K. Baldridge, J. A. Boatz, J. H. Jensen, S. Koseki, M. S. Gordon, K. A. Nguyen, T. L. Windus, and S. T. Elbert, *Quantum Chem. Prog. Exchange Bull.* **10**, 52 (1990).
- [22] R. R. Lucchese, G. Raseev, and V. McKoy, *Phys. Rev. A* **26**, 1406 (1982).
- [23] R. B. Singh and D. K. Rai, *J. Mol. Spectrosc.* **19**, 424 (1966).
- [24] K. P. Huber and G. Herzberg, *Constants of Diatomic Molecules* (Van Nostrand Reinhold, New York, 1979).
- [25] Jeffrey A. Nichols, Danny L. Yeager, and Poul Jørgensen, *J. Chem. Phys.* **80**, 293 (1984).
- [26] T. N. Resigno, A. Gerwer, B. V. McKoy, and P. W. Langhoff, *Chem. Phys. Lett.* **66**, 116 (1979).